Research Article Vol. 4, No. 6 / June 2017 / Optica 605

Miniature wide-spectrum mode sorter for vortex beams produced by 3D laser printing

Shlomi Lightman,[1,2,*] Gilad Hurvitz,[1] Raz Gvishi,[1] and Ady Arie[2]

[1]Applied Physics Division, Soreq NRC, Yavne 81800, Israel
[2]School of Electrical Engineering, Tel Aviv University, Tel-Aviv 69978, Israel
*Corresponding author: shlomili@soreq.gov.il

Received 9 March 2017; revised 7 May 2017; accepted 7 May 2017 (Doc. ID 290347); published 2 June 2017

Optical vortex beams can be used as carriers of information in optical communication and quantum optics applications. Owing to their spatial orthogonality, these beams can be multiplexed and demultiplexed, but up until now this was primarily achieved by bulky and large devices. In this work, a new approach is used to fabricate miniature vortex mode sorters based on three-dimensional laser printing, thereby enabling direct integration into optical systems. Mode sorters that are composed of two separate elements as well as a single integrated device are presented. These devices can handle both pure and mixed vortex beams with topological charge $|l| \leq 3$ and $|l| \leq 2$ for the dual-element device and integrated system, respectively. Mode-sorter spectral bandwidth and surface-quality effects are also discussed.

OCIS codes: (140.3490) Lasers, distributed-feedback; (060.2420) Fibers, polarization-maintaining; (060.3735) Fiber Bragg gratings; (060.2370) Fiber optics sensors.

https://doi.org/10.1364/OPTICA.4.000605

1. INTRODUCTION

Optical vortex beams are characterized by a helical wavefront. Their azimuthal phase dependence is $\exp(i\ell\phi)$, where ℓ, the topological charge, is an integer and ϕ is the transverse azimuthal angle. It was shown by Allen *et al.* [1] that these beams can carry orbital angular momentum (OAM) of $\ell\hbar$ per photon, where $\hbar$ is the reduced Planck constant. Optical vortex beams have attracted intense attention in recent years and have been studied in various applications, including particle manipulation [2], microfabrication [3], astronomy [4], quantum optics [5], high-resolution microscopy [6], and space-division multiplexed communication systems [7]. The Laguerre–Gaussian family of beams is an example of a set of vortex beams that are also solutions of the paraxial Helmholtz equation. In this case, beams with different ℓ values are orthogonal, and hence they can be spatially multiplexed and demultiplexed on the same physical channel. These beams can then be used as carriers of information, thereby increasing information capacity of an optical communication channel [8]. Multiplexing of vortex beams is also beneficial for quantum information applications [9].

Berkhout *et al.* [10] have demonstrated an innovative method for multiplexing OAM states by applying a Cartesian to log-polar transformation. This transformation maps the azimuthal phase profile of an OAM mode into a tilted planar wavefront. As a result, linear combination of OAM states can be simultaneously transformed into a set of planar waves with tilted wavefronts, where the tilt angle depends on the topological charge. These tilted waves can therefore be easily separated in the far field by a lens. The Cartesian to log-polar transformation is based on two diffractive optical elements. The first element maps the coordinates of the incoming beam (in the x–y plane) to an output plane (u–v) by the relations

$$u = -a \ln\left(\sqrt{x^2 + y^2}/b\right), \tag{1}$$

$$v = a \times \tan^{-1}(y/x). \tag{2}$$

Here, the coordinates u and v are the Cartesian coordinates in the Fourier plane of the first element. Parameter a is defined as $a = d/2\pi$, where d is the width of the second element. The parameter b determines the tilt of the transformed beam along the v axis. The mapping process of the first element adds distortions to the beam's phase, which are then corrected by the second element [11].

The height profiles of the two diffractive elements, Z_1 and Z_2, are [12]

$$Z_1(x,y) = \frac{a}{f(n_m - n_{\text{air}})}\left[y \arctan(y/x) - x \ln\left(\frac{\sqrt{x^2+y^2}}{b}\right) + x - \frac{1}{2a}(x^2+y^2)\right], \tag{3}$$

$$Z_{2(x,y)} = -\frac{ab}{f(n_m - n_{\text{air}})}\left[\exp(u/a) \times \cos(v/a) - \frac{1}{2ab}(u^2+v^2)\right], \tag{4}$$

where n_m and n_{air} are the element and air refractive indices, and f is the distance between the two elements, which is also the focal length of the integrated lens terms in Eqs. (3) and (4). After propagating through the two surfaces, each beam with a topological charge ℓ accumulates a gradient phase of $2\pi\ell$ along the x direction. The separation distance (Δ_x) between modes at the focal plane is dictated by ℓ and given by

$$\Delta_x = \ell \times \left(\frac{f\lambda}{d}\right). \tag{5}$$

Until now, the two-element OAM mode (de)multiplexer was demonstrated either by two spatial light modulators (SLMs) [10], or by large scale (>mm–cm) elements made by CNC milling methods [7] or diamond turning [12]. The latter approach was also used for mode-division multiplexing in a few-mode optical fiber system [13]. Recent work also demonstrated diffractive elements based on log-polar transformation using electron-beam lithography [14,15] in addition to an integrated, single millimeter-scale diffractive device. These methods work well for laboratory applications; however, they require additional bulk optics devices such as lenses and mirrors, as well as a significant working space (>mm) between the elements. The diffractive optical elements [14,15] are wavelength dependent and hence have limited bandwidth. Finally, it is difficult to integrate these bulky mode sorters directly into optical systems, e.g., at the tip of the optical fiber [16] or at the exit facets of lasers [17] or nonlinear optical crystals [18].

A new fabrication method for a vortex (de)multiplexer is introduced here by a 3D-direct laser writing (3D-DLW) [19] system. The concept of DLW enables printing of arbitrary shapes by polymerization of a light-sensitive material volume (Voxel) by a nonlinear two-photon absorption mechanism [20]. This method can fabricate micro-optical elements at the tips of optical fibers [21], in free space [22], or directly on nonlinear crystal facets [23]. Using the DLW process, we demonstrate here micrometer-scale (de)multiplexers. Furthermore, we demonstrate capabilities that are not possible in alternative fabrication technologies [7,12] by fabricating a compact integrated vortex (de)multiplexer, where the distance and relative position of the two elements are already defined during the fabrication process. This may open new and exciting possibilities for integrated optics devices for communication systems, quantum optics, non-linear optics, and more.

2. METHODS

A. Design

A simulation code based on split-step Fourier method [24] was used to study OAM beam propagation and optimize the design. Furthermore, by fine-tuning the phase elements, precise wave fronts were produced, helping to increase the OAM states' sorting capability. Optimal profiles were calculated, leading to parameter values of $a = 19$ μm and $b = 25$ μm [see Eqs. (3) and (4)]. The lateral dimensions of the first and second elements were designed to be 70×70 μm and 160×95 μm, with max heights of 12.5 and 20.4 μm, respectively. The distance between the two elements was 0.8 mm. Designed structures can be seen in Figs. 1(a) and 1(b). We note that systems of this size suffer from transformation errors and increased crosstalk when introducing higher OAM modes. This happens when the skew angle of the vortex beams, ℓ/kr, dominates over the angular deviation

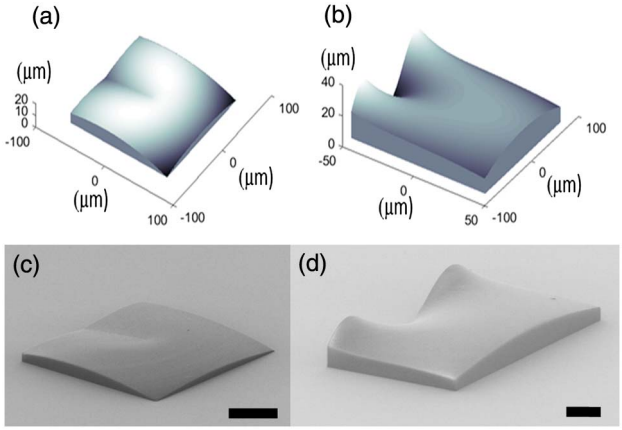

Fig. 1. Top: Theoretical (de)multiplexer designs of the (a) transforming and (b) correcting elements. Bottom: (c, d) SEM images of the above-fabricated elements. Scale bars are 25 μm.

introduced by the (de)multiplexer, r/f, for small angles. Here, $k = 2\pi/\lambda$ is the light wavenumber and r symbolizes the beam's radius. Hence, the system's performance is governed by the number of states: $\ell \ll 2\pi r^2/f\lambda$. This expression is the Fresnel number divided by 2π [25]. In our case, the topological charge that can be processed should be smaller than 5. This can be further increased either by increasing the beam width and system dimensions or by reducing the distance between the two elements, as will be shown subsequently for the case of an integrated (de)multiplexer.

B. Fabrication

The mode-sorting elements were fabricated by 3D-DLW using a commercial femtosecond laser lithography system (Photonic Professional GT, Nanoscribe GmbH, Germany). The complete optical system was manufactured from one single material. We used a negative photoresist that exhibited high optical quality (IP-S, Nanoscribe, GmbH). The refractive index of this optical material is ~1.51 for 780 nm wavelength. A drop of the photoresist was placed on a square glass; then, by exposing it to femtosecond pulses, the two-photon signal induced local polymerization of the photoresist as the laser scanned through its volume.

The designed structures were printed layer by layer with a distance of 100 nm between consecutive layers. After the printing process, the elements were rinsed in a developer (mr-dev 600 for IP-photoresist) resin for 30 min, followed by a short, subsequent rinsing of isopropanol for leftover removal. Figures 1(c) and 1(d) display the final outcome of the printed elements as they were characterized by SEM. We also fabricated a single, integrated device as will be described in Section 3.C.

C. Optical Characterization

In order to study demultiplexing performance, we generated different optical vortex beams. Here we tested the demultiplexing capabilities, but, owing to symmetry consideration, the same performance is expected when the device is used as a multiplexer. A Mai Tai Ti:sapphire oscillator laser (Spectra-Physics, USA) with 690–1040 nm tunable range was used in its CW mode (i.e., narrow and well-defined spectral emission). A phase-only reflective SLM (PLUTO-NIR-011, HOLOEYE, USA) was programmed

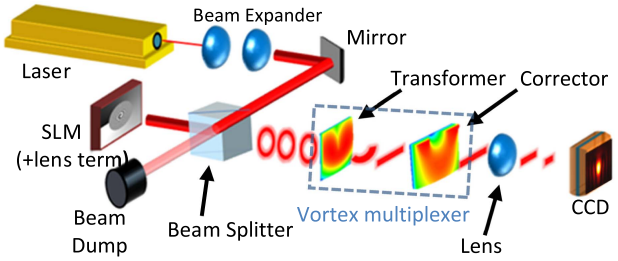

Fig. 2. Schematic design of the optical setup for testing the vortex multiplexer.

to spatially modulate the phase of the beam, followed by an additional lens term that focused the beam into the (de)multiplexer (Fig. 2). A Gaussian beam was focused ($f = 160$ mm, N.A. $= 0.01$) to a 56 μm spot size ($1/e^2$), i.e., about ~50 times larger than the wavelength, and hence the experimental setup is well within the paraxial approximation.

3. RESULTS

A. Separated System

Various vortex beams carrying different OAM values $-3\hbar \leq \ell\hbar \leq 3\hbar$ were generated by the SLM. The transformed and then corrected beams were detected by an imaging system and CCD. By setting the $\ell = 0$ state as a reference, higher modes could then be analyzed according to their transverse location on the CCD. Figure 3 shows (top row) the simulated beams entering the first element of the mode sorter. Brightness and colors refer, respectively, to intensity and phase of each beam. Simulated intensity at the detector's plane can be seen in the center part of Fig. 3. The corresponding experimental results are shown in the bottom row of Fig. 3. The calculated and measured results have good agreement, and Δ_x was measured to be 9.4 μm per angular momentum unit. Additional fringes appear in the measured output beams, with respect to simulated calculations. This may be due to the measuring system's optical surface quality and the SLM pixelated arrays.

In the next step, mixed states carrying simultaneously different values of OAM were generated in order to evaluate the demultiplexer crosstalk. Two examples of mixed states with (1) $\ell = -1$ and $\ell = 2$ and (2) $\ell = \pm 2$ are shown in Fig. 4. The left column

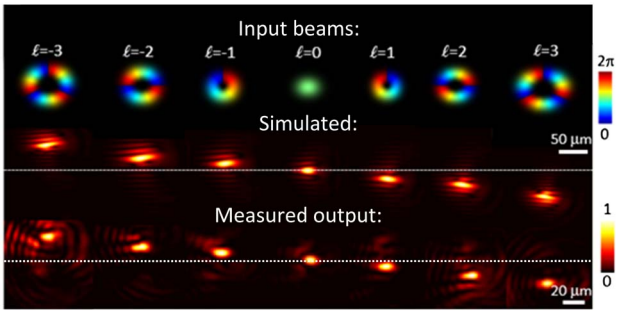

Fig. 3. Top row: incoming vortex beams towards the mode sorter. Center row: simulated beams at detector. Bottom row: measured beams at detector. The dotted horizontal lines mark the location of the $\ell = 0$ beam. Upper and lower scale bars correspond to the incoming and focused demultiplexed beams, respectively.

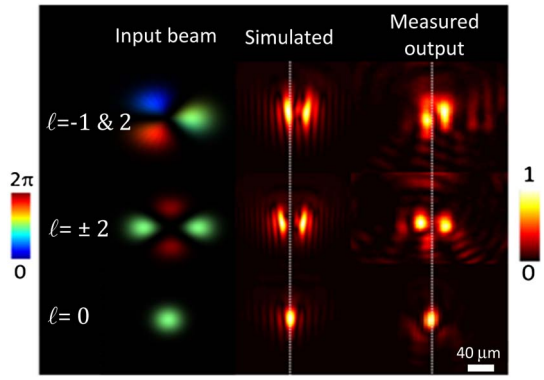

Fig. 4. Left column: interference of various states before entering the mode sorter. Middle column: simulated spots at detector. Right column: measurements. The bottom $\ell = 0$ row is for reference.

of Fig. 4 shows the simulated beams just before they enter the first demultiplexer element. Calculated and measured spots are shown in the middle and right columns, respectively.

The demultiplexer height profiles [Eqs. (3) and (4)] are wavelength independent. This achromatic performance originates from the phase functions of the two elements, which are inversely proportional to the wavelength that is canceled when transforming from the phase functions to the height profile expressions. The relation between the thickness and accumulated phase is [26]

$$h(x, y) = \frac{\varphi(x, y) \times \lambda}{2\pi(n_m - n_{\text{air}})}. \quad (6)$$

This means that the mode-sorter performance is essentially independent of the beam's wavelength. However, this is not exactly the case since the material's dispersion would still induce a wavelength-dependent phase.

In order to investigate the mode sorter's spectral bandwidth, an interference of OAM beams of $\ell = 1$ and $\ell = -1$ (which can be also described as a first-order Hermite–Gaussian mode) was introduced to the mode sorter. We repeated this experiment at four different wavelengths: 690, 790, 890, and 990 nm. Analysis of the resulting spots showed that the OAM states can be resolved and separated, as seen in Fig. 5(a). Furthermore, by line-scanning the center of the spots [Fig. 5(b)], it is possible to determine the separation distances with correlation to the operating wavelengths [Fig. 5(c)]. The line scan for 690 nm wavelength in Fig. 5(b) has a side peak which appears due to an adjacent fringe. The results show that the separation distance is linearly dependent on the wavelength [Eq. (5)]. These results show good agreement with the theoretical calculation illustrated in Fig. 5(c). The bandwidth of the device is therefore at least 300 nm, and is limited by the dispersion of the photoresist. By tailoring the design, it is possible to realize mode sorting at other wavelengths in the range ~300–2000 nm. Outside this region the polymer is not transparent, and it would be necessary to use other suitable materials.

B. Surface Quality Effects

We have found by both simulations and experiments that the performance of the mode (de)multiplexer depends critically on the surface quality of the facets of its two elements. Prototypes were printed under different conditions, and their surface roughness and theoretical functionality were analyzed.

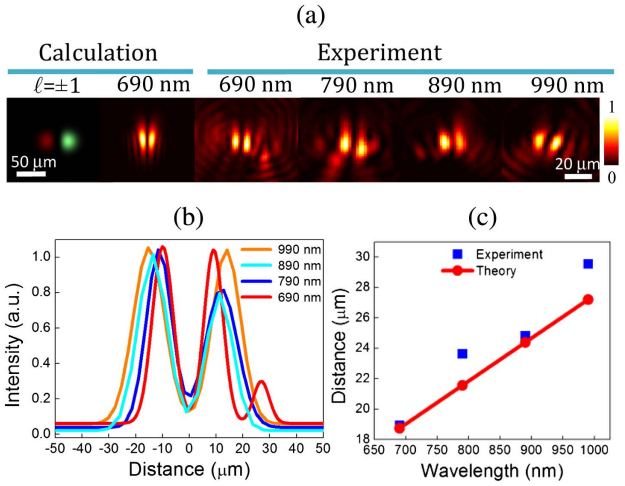

Fig. 5. Wavelength dependency measurements of incoming $\ell = \pm 1$ interference beam. (a) Simulated and measured beams at the detector plane, when varying the beam's wavelength from 690 to 990 nm. Left and right scale bars correspond to the incoming beam and focused demultiplexed beams, respectively. (b) Line-scans of the measured spots at various wavelengths. (c) Peak-to-peak distances of measured and calculated values between the OAM states at different wavelengths.

Here we introduce three of those cases, which exhibit different levels of optical surface quality. This study focuses mainly on the transforming element (i.e., first element). The first case is an IP-DIP (negative) photosensitive printed element (Nanoscribe GmbH, Germany), with a designed 200 nm distance between fabricated layers. Here, each layer has a fixed height (Z) value. In the second case, the IP-DIP was used to print surface contours, so each layer is described by a varying height surface of $Z(x, y)$. The distance between each layer was set to 200 nm. The third case is a polymerized IP-S structure, when each layer had a fixed height and differed by 200 nm from the next layer. All the printed elements were designed with lateral dimension of 60 × 60 μm and maximum height of 27 μm. Figure 6 shows SEM pictures of side

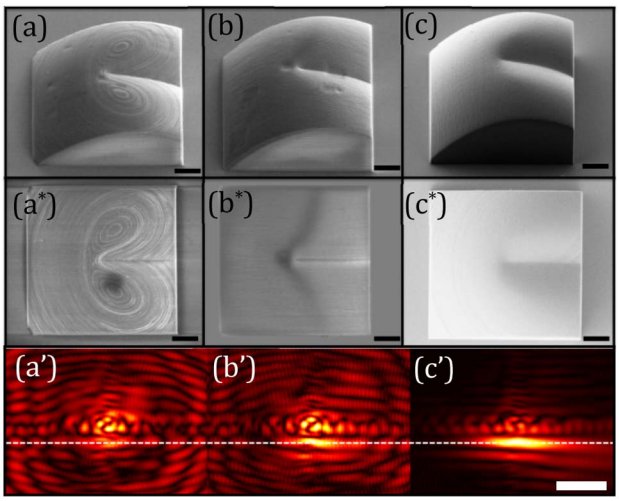

Fig. 6. SEM pictures of side (top row) and top (center row) views of three printing methods, which resulted in estimated surface roughness of (a) 450, (b) 250, and (c) 50 nm. Bottom row: Simulated $\ell = 2$ vortex beams at the detector plane for the three samples. The dotted horizontal lines mark the location for the $\ell = 2$ beam. Scale bars are 10 μm.

(a, b, c) and top (a^*, b^*, c^*) views of the mentioned cases. The surface profiles were measured using an optical profiling system (Wyko, NT9100, Veeco). Peak-to-valley values of the structures in Figs. 6(a), 6(b), and 6(c) were 450, 250, and 50 nm, respectively. These values were implemented in theoretical calculation to analyze the correlation between the surface optical quality and the demultiplexed OAM ($\ell = 2$) beam on the detector. The results are illustrated in Figs. 6(a′)–6(c′). The dotted horizontal lines mark the location for the $\ell = 2$ state. Accurate production combined with smoother surface profiles clearly exhibits lower side-lobes and reduces crosstalk. We note that all the experimental results shown in Section 3.A fit the surface quality properties related to the structure shown in Fig. 6(c). The ratios between the energy in the central lobe and the total energy on the detector were calculated. These values are 1%, 2%, and 8%, which correspond to the calculated spatial energy distributions in Figs. 6(a′), 6(b′), and 6(c′), respectively.

C. Integrated System

Direct laser-printed micro-scale mode sorters are fairly small and have the potential to be integrated easily in many optical applications, such as optical fibers [24], nonlinear crystals [23], laser amplifiers, and micro-optical systems. In order to demonstrate the new possibilities that are now enabled by laser printing, we fabricated a combined system in which the two elements are positioned with the right spacing. In this case the alignment spacers were part of the fabrication process, as seen in Fig. 7. This integrated sorter was fabricated in a single, continuous printing process using the IP-DIP photoresist. It is important to emphasize that a fabrication of an integrated mode sorter cannot be done by other methods that were used so far, such as diamond turning [12] or CNC milling [7]. The distance between each printed layer of the elements was chosen to be 200 nm. The lateral dimensions of the transformer and corrector were 60 × 60 μm and 60 × 30 μm, with maximum heights of 32 and 51.5 μm, respectively. The axial distance between the element bases was calculated to be 60 μm. This device saves the need for careful alignment and positioning of the two separate elements. Furthermore, the distance between the two elements is more than an order of magnitude shorter with respect to the mode sorter that was described previously. The Fresnel number of this integrated system, which is inversely proportional to this distance, is quite large (~21). This means that this smaller and more precise system can potentially accommodate vortex beams up to a charge of 10. This value might be

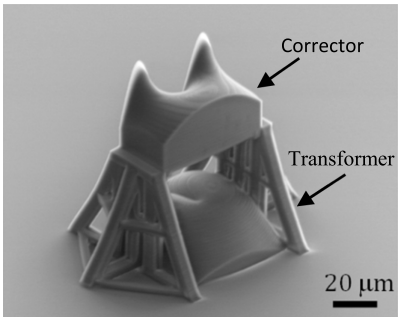

Fig. 7. SEM picture of a combined mode sorter. The transformer and corrector elements are integrated on a glass substrate. The relatively massive poles are needed for accurate alignment.

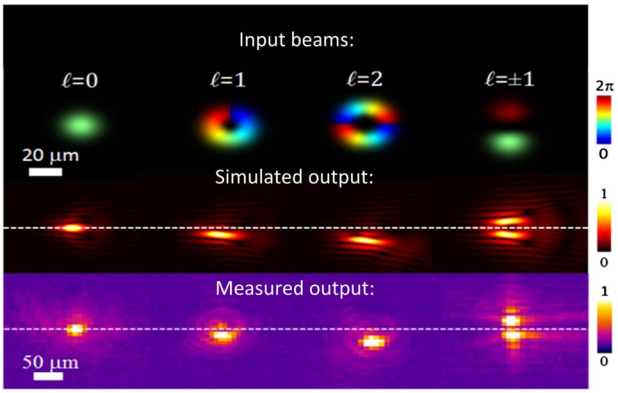

Fig. 8. Top row: Input beams. Center row: simulated output beams. Bottom row: measured output beams. The dotted horizontal lines mark the location of the $\ell = 0$ beam. Upper and lower scale bars correspond to the incoming and focused demultiplexed beams, respectively.

achieved for a printed element of high optical surface quality but, with the current surface fabrication quality, we limited our tests up to a charge of 2. In order to test the optical performance of the combined system, we used a 1550 nm fiber laser (FLS 2600, EXFO, Canada) that was collimated to a waist diameter of 1.8 mm. This beam was then converted into different types of OAM beams using a phase plate glass matrix (VPP-m1550, RPC Photonics, USA). A Fourier lens with a focal length of 25.4 mm was used to bring the vortex beams into the combined mode sorter. After propagating through the two elements, the beams were detected by a short-wavelength IR camera (Xenics, Xeva-1.7-640, Belgium). In addition to these pure OAM states, a mixed state of $\ell = \pm 1$ was produced by inserting a 170 μm thick glass in the center of the beam. One half of the beam travels through the glass, which adds a π-shift to its phase (modulo an integer number of 2π phase) with respect to the other half of the beam that travels in air. A slight tilt of the glass was needed for phase adjustment. This generates a Hermite-Gaussian$_{01}$-like mode, which can be decomposed into two vortex beams with topological charges of +1 and −1. A 1550 nm wavelength was used to overcome the moderate optical quality of the fabricated surfaces. This approach enabled successive measurements of 0, $1\hbar$, $2\hbar$, and $-1\hbar$ OAM values. The experimental results are shown in Fig. 8. The modes were easily resolved and the separation coefficient Δ_x was measured to be 28.5 μm per angular momentum unit. This system can potentially detect and demultiplex higher OAM states, as the optical quality of the fabricated surfaces is increased.

4. SUMMARY

We have fabricated, by direct laser printing, functional 3D micrometer-scale (de)multiplexing devices which can either combine or separate OAM states in two approaches. In the first approach, the (de)multiplexer consisted of two diffractive phase elements, while, in the latter approach, an integrated and fully aligned system combined the two diffractive elements into one compact and stable device. We were able to differentiate single and mixed OAM states in the range $-3 \le \ell \le 3$. In the case of two separated elements and in the case of an integrated system, we managed to separate pure OAM states up to a topological charge of 2, as well as mixed OAM states. These devices can potentially (de)multiplex vortex beams with even higher topological charge, provided that the surface quality can be improved. The spectral bandwidth of the mode sorter was measured to be 300 nm, limited by the dispersion of the photoresist.

Acknowledgment. We thank the Karlsruhe Nano Micro Facility (KNMF, https://www.kit.edu/knmf) of the Forschungszentrum Karlsruhe for provision of access to instruments at their laboratories, and we would like to thank S. Hengsbach for the 3D-DLW sample fabrications. We also thank the Brojde Center at the Hebrew University of Jerusalem for the use of the 3D-DLW Nanoscribe system.

REFERENCES

1. L. Allen, M. W. Beijersbergen, R. J. C. Spreeuw, and J. P. Woerdman, "Orbital angular momentum of light and the transformation of Laguerre–Gaussian laser modes," Phys. Rev. A **45**, 8185–8189 (1992).
2. V. Garcés-Chávez, D. McGloin, M. Padgett, W. Dultz, H. Schmitzer, and K. Dholakia, "Observation of the transfer of the local angular momentum density of a multiringed light beam to an optically trapped particle," Phys. Rev. Lett. **91**, 093602 (2003).
3. J. Hamazaki, R. Morita, K. Chujo, Y. Kobayashi, S. Tanda, and T. Omatsu, "Optical-vortex laser ablation," Opt. Express **18**, 2144–2151 (2010).
4. G. A. Swartzlander, E. L. Ford, R. S. Abdul-Malik, L. M. Close, M. A. Peters, D. M. Palacios, and D. W. Wilson, "Astronomical demonstration of an optical vortex coronagraph," Opt. Express **16**, 10200–10207 (2008).
5. J. García-Escartín and P. Chamorro-Posada, "Quantum multiplexing with the orbital angular momentum of light," Phys. Rev. A **78**, 062320 (2008).
6. S. W. Hell and J. Wichmann, "Breaking the diffraction resolution limit by stimulated emission: stimulated-emission-depletion fluorescence microscopy," Opt. Lett. **19**, 780–782 (1994).
7. Y. Yan, G. Xie, M. P. J. Lavery, H. Huang, N. Ahmed, C. Bao, Y. Ren, Y. Cao, L. Li, Z. Zhao, A. F. Molisch, M. Tur, M. J. Padgett, and A. E. Willner, "High-capacity millimetre-wave communications with orbital angular momentum multiplexing," Nat. Commun. **5**, 4876 (2014).
8. G. Gibson, J. Courtial, M. J. Padgett, M. Vasnetsov, V. Pas'ko, S. M. Barnett, and S. Franke-Arnold, "Free-space information transfer using light beams carrying orbital angular momentum," Opt. Express **12**, 5448–5456 (2004).
9. M. N. O'Sullivan, M. Mirhosseini, M. Malik, and R. W. Boyd, "Near-perfect sorting of orbital angular momentum and angular position states of light," Opt. Express **20**, 24444–24449 (2012).
10. G. Berkhout, M. Lavery, J. Courtial, M. Beijersbergen, and M. J. Padgett, "Efficient sorting of orbital angular momentum states of light," Phys. Rev. Lett. **105**, 153601 (2010).
11. W. J. Hossack, A. M. Darling, and A. Dahdouh, "Coordinate transformations with multiple computer-generated optical elements," J. Mod. Opt. **34**, 1235–1250 (1987).
12. M. P. J. Lavery, D. J. Robertson, G. C. G. Berkhout, G. D. Love, M. J. Padgett, and J. Courtial, "Refractive elements for the measurement of the orbital angular momentum of a single photon," Opt. Express **20**, 2110–2115 (2012).
13. H. Huang, G. Milione, M. P. J. Lavery, G. Xie, Y. Ren, Y. Cao, N. Ahmed, T. A. Nguyen, D. A. Nolan, M. J. Li, M. Tur, R. R. Alfano, and A. E. Willner, "Mode division multiplexing using an orbital angular momentum mode sorter and MIMO-DSP over a graded-index few-mode optical fibre," Sci. Rep. **5**, 14931 (2015).
14. G. Ruffato, M. Massari, and F. Romanato, "Compact sorting of optical vortices by means of diffractive transformation optics," Opt. Lett. **42**, 551–554 (2017).
15. G. Ruffato, M. Massari, G. Parisi, and F. Romanato, "Test of mode-division multiplexing and demultiplexing in free-space with diffractive transformation optics," Opt. Express **25**, 7859–7868 (2017).
16. T. Gissibl, S. Thiele, A. Herkommer, and H. Giessen, "Two-photon direct laser writing of ultracompact multi-lens objectives," Nat. Photonics **10**, 554–560 (2016).

17. J. Look, S. Einfeldt, O. Kruger, V. Hoffmann, A. Knauer, M. Weyers, P. Vogt, and M. Kneissl, "Laser scribing for facet fabrication of InGaN MQW diode lasers on sapphire substrates," IEEE Photon. Technol. Lett. **22**, 416–418 (2010).
18. A. Shapira, A. Libster, Y. Lilach, and A. Arie, "Functional facets for nonlinear crystals," Opt. Commun. **300**, 244–248 (2013).
19. A. Selimis, V. Mironov, and M. Farsari, "Direct laser writing: principles and materials for scaffold 3D printing," Microelectron. Eng. **132**, 83–89 (2015).
20. R. L. Sutherland, *Handbook of Nonlinear Optics* (Marcel Dekker, 1996).
21. G. Cojoc, C. Liberale, P. Candeloro, F. Gentile, G. Das, F. D. Angelis, and E. D. Fabrizio, "Optical micro-structures fabricated on top of optical fibers by means of two-photon photopolymerization," Microelectron. Eng. **87**, 876–879 (2010).
22. A. Zukauskas, M. Malinauskas, and E. Brasselet, "Monolithic generators of pseudo-nondiffracting optical vortex beams at the microscale," Appl. Phys. Lett. **103**, 181122 (2013).
23. S. Lightman, R. Gvishi, G. Hurvitz, and A. Arie, "Shaping of light beams by 3D direct laser writing on facets of nonlinear crystals," Opt. Lett. **40**, 4460–4463 (2015).
24. O. V. Sinkin, R. Holzlohner, J. Zweck, and C. R. Menyuk, "Optimization of the split-step Fourier method in modeling optical-fiber communications systems," J. Lightwave Technol. **21**, 61–68 (2003).
25. M. P. J. Lavery, D. J. Robertson, A. Sponselli, J. Courtial, N. K. Steinhoff, G. A. Tyler, A. E. Willner, and M. J. Padgett, "Efficient measurement of an optical orbital-angular-momentum spectrum comprising more than 50 states," New J. Phys. **15**, 013024 (2013).
26. B. E. A. Saleh and M. C. Teich, *Fundamentals of Photonics* (Wiley, 1991).